Generated Pattern Current for Anodizing: Pore Ordering, Oxide Morphology Control, and Thermal Stabilization in Anodic Alumina and Titanium Oxide Formation

Ibrahim Karakoc

GigaPulse Energy, Izmir, Turkey

ibrahim@gigapulse.energy

PCT/TR2025/051176 | USPTO Appl. No. 19/298,223 | Priority Date: July 23, 2025

Abstract

Anodizing of aluminum and titanium produces functional oxide layers whose properties—pore diameter, interpore distance, ordering degree, barrier layer thickness, and thermal stability—are determined by three concurrent physical processes: field-assisted oxide formation and dissolution at the metal–electrolyte interface, pore self-ordering kinetics driven by mechanical stress and electric field distribution, and Joule heating that limits maximum current density and risks burning under constant current conditions. Conventional constant current (CC) or constant voltage (CV) anodizing applies temporally invariant electrical conditions that cannot independently optimize these three processes; the result is suboptimal pore ordering, variable oxide morphology, and burning risk at elevated current densities. This paper presents the application of the Generated Pattern Current (GPC) paradigm, implemented through the Dynamic Defined Pattern Charging (DDPC) framework, to anodizing. GPC applies a three-phase temporal current structure: a high-current oxide growth phase, a mid-current dissolution balance phase, and a low-current thermal relaxation and self-ordering phase. Jensen's inequality applied to the nonlinear field-assisted oxide dissolution kinetics formally establishes that temporally structured current produces different time-averaged oxide morphology than equivalent CC conditions. Predictions include improved hexagonal pore ordering, narrowed pore diameter distribution, suppressed burning at high current densities, and accelerated hard anodizing compared to CC baselines. The GigaPulse Lab reference implementation provides closed-loop thermal index monitoring and adaptive pattern control without hardware replacement of existing anodizing power supplies. The viscous flow model of pore growth [26] and the fluoride-mediated dissolution mechanism in titanium anodizing [27, 28] are incorporated as the governing physical framework, superseding the classical field-assisted dissolution model where current evidence requires.

Keywords: *Generated Pattern Current (GPC); Dynamic Defined Pattern Charging (DDPC); anodizing; anodic alumina; porous anodic alumina (PAA); self-ordering; pore ordering; oxide morphology; Joule heating; hard anodizing; titanium anodizing; barrier layer; viscous flow model; TiO_2 nanotubes*

1. Introduction

1.1 Anodizing and Functional Oxide Applications

Anodizing is an electrochemical surface treatment in which a metal anode—most commonly aluminum or titanium—is oxidized in an acidic electrolyte to form a controlled oxide layer. For aluminum, the resulting anodic alumina (AAO) has been studied extensively

since Keller et al. first characterized its porous structure [13]; the discovery by Masuda and Fukuda of conditions yielding self-ordered hexagonal pore arrays [2] transformed AAO from an industrial coating into a nanofabrication template with applications in magnetic storage media [8], photonic crystals [11], drug delivery membranes, and nanowire synthesis [12]. For titanium, anodizing produces TiO_2 nanotube arrays with applications in photocatalysis, biomedical implants, and dye-sensitized solar cells [5, 22].

The properties of the anodic oxide that determine functional performance are: pore diameter dp and interpore distance Dint (which determine template geometry for nanofabrication), ordering degree expressed through the fraction of hexagonally coordinated pores θhex, barrier layer thickness db (which determines ionic transport resistance and capacitive properties), and structural uniformity along the pore axis. All five properties are sensitive to the anodizing current density and its temporal structure [3, 5, 7, 14].

1.2 Physical Mechanisms Governing Pore Growth: Viscous Flow and Dissolution Models

The mechanism by which ordered porous structures develop during anodizing has been revised substantially in recent decades. The classical field-assisted dissolution model has been challenged and partially supplanted by the viscous flow model proposed by Garcia-Vergara et al. [26]. In the viscous flow model, oxide material generated at the metal–oxide interface migrates plastically toward the pore walls under the mechanical stress induced by volume expansion during $Al \rightarrow Al_2O_3$ conversion (Pilling–Bedworth ratio ≈1.3). Pore formation and elongation arise from this viscous flow of oxide rather than from dissolution, which explains the mass balance discrepancy observed under the classical model.

For titanium anodizing in fluoride-containing electrolytes, the formation of TiO_2 nanotube arrays involves a mechanistically distinct process. Zhuang et al. [27] demonstrated that fluoride ions play a dual role: they complex Ti^{4+} ions at the tube bottom to enable field-assisted dissolution of TiO_2, and they facilitate plastic flow of the partially fluorinated oxide at the pore walls. The work of Li et al. [28] further clarified that the pore growth rate is primarily controlled by the oxide formation rate at the barrier layer rather than by dissolution at the pore tip. These mechanistic refinements identify the barrier layer formation kinetics—rather than dissolution kinetics—as the primary target for temporal current structuring.

1.3 Three Efficiency-Limiting Phenomena in Anodizing

Field-assisted oxide formation and dissolution are concurrent competing processes at the metal–oxide and oxide–electrolyte interfaces respectively [3, 13, R1]. The steady-state pore geometry reflects the balance between these two processes: the barrier layer thickness $db \approx kV$ (where $k \approx 1.2$ nm/V for aluminum in sulfuric acid) is established at the voltage where the formation and dissolution rates are equal [3, 13].

Pore self-ordering arises from the mechanical stress field generated by the volume expansion during $Al \rightarrow Al_2O_3$ conversion [4, 9, R1]. Adjacent growing pores repel through the compressive stress field, driving hexagonal ordering with interpore distance Dint ≈2.5 nm/V [10]. Self-ordering is a kinetic process that requires sustained, uniform electrical conditions over timescales comparable to the pore initiation and stabilization time; non-uniform current

distribution or current transients interrupt the ordering kinetics and produce disordered regions [9, 15].

Joule heating is the primary operationally limiting phenomenon in hard anodizing where current densities up to 150–200 mA/cm² are desired [6]. The oxide layer has substantially higher electrical resistance than the electrolyte, and the power dissipated $P_{Joule} = j^2 \cdot R_{oxide}$ generates local temperature increases $\Delta T \propto j^2$ that destabilize the oxide dissolution–formation balance and at sufficient current density lead to burning—runaway local oxide dissolution that destroys the anodic film [7, 12].

1.4 Limitations of CC and CV Anodizing

CC anodizing applies a fixed current density that simultaneously drives oxide formation, dissolution, and Joule heating. These three processes cannot be independently controlled: high current density simultaneously accelerates oxide growth and Joule heating, limiting the maximum usable current density and therefore the maximum achievable growth rate in hard anodizing [6]. CV anodizing provides some intrinsic self-limitation through the resistance-driven current decay, but neither CC nor CV provides a mechanism for periodically allowing thermal relaxation while maintaining oxide growth over the longer timescale. Pulsed anodizing has been explored for hard anodizing [6, 15], but fixed-parameter pulse protocols do not adapt to the evolving oxide state and do not provide independent control over the formation-dissolution balance and self-ordering kinetics.

1.5 GPC as Temporal Current Design for Anodizing

Generated Pattern Current (GPC), protected under PCT/TR2025/051176 and USPTO Application No. 19/298,223 (priority date July 23, 2025), applies temporally structured current I(t) to the anodizing cell. The theoretical foundation derives from Jensen's inequality applied to the nonlinear field-assisted oxide kinetics:

$$f(\bar{I}) \neq \langle f(I(t)) \rangle$$

where f represents any nonlinear anodizing response. The total oxide thickness grown depends on the total charge passed $Q = \langle I \rangle \cdot t$, so GPC preserves the oxide growth rate at equal average current while changing the temporal distribution to control morphology and thermal conditions.

Section 2 presents the anodizing electrochemical physics incorporating current mechanistic understanding. Section 3 analyzes the three GPC morphology control mechanisms. Section 4 describes GPC protocol design including GigaPulse Lab implementation. Section 5 addresses aluminum and titanium technology-specific considerations. Section 6 quantifies expected outcomes. Section 7 presents the experimental validation framework. Section 8 discusses implications. Section 9 concludes.

2. Anodizing Electrochemical Physics

2.1 Oxide Formation Reactions and Faradaic Relationship

The anodizing reaction for aluminum in acidic electrolyte proceeds through two competing paths [3, 13]:

$$2Al + 3H_2O \rightarrow Al_2O_3 + 6H^+ + 6e^- \quad \textit{(barrier oxide formation)}$$

$Al_2O_3 + 6H^+ \rightarrow 2Al^{3+} + 3H_2O$ *(chemical dissolution)*

The net oxide thickness grown per unit time is proportional to the difference between the formation rate (which scales with current density j) and the dissolution rate (which scales with local temperature and electrolyte concentration). Under the viscous flow model [26], a significant fraction of the oxide formed at the barrier layer migrates laterally as viscous flow to compose the pore walls, meaning the formation rate at the barrier layer—rather than the dissolution rate at the pore tip—is the primary kinetic variable controlled by GPC.

2.2 Barrier Layer Dynamics and Field-Assisted Growth

The barrier layer at the base of each pore is the active growth zone. Its thickness db adjusts to maintain the high electric field E = Vbarrier/db ≈10^9 V/m that drives ionic transport. In steady-state CC anodizing, db ≈ k·Vcell giving the empirical relationship Dint ≈2.5·db for hexagonally self-ordered structures [10, 13].

The field-assisted ionic transport through the barrier layer is described by the high-field conduction model:

$j = j_0 \cdot \exp(\beta E) = j_0 \cdot \exp(\beta\, Vbarrier / db)$

The exponential nonlinearity means that Jensen's inequality applies: a temporally structured current that produces the same time-averaged j but varies between high and low values produces a different time-averaged field distribution across the barrier layer than constant j at the mean value. This is the fundamental mechanism by which GPC modifies oxide morphology without changing the total oxide volume grown.

2.3 Self-Ordering Kinetics and the Hexagonal Instability

The mechanical stress model for pore self-ordering [4, 9, R1] predicts that the equilibrium interpore distance Dint corresponds to the voltage V at which the compressive stress from volume expansion is exactly balanced by the tensile stress from the electric field at the pore walls. At this optimal voltage, the hexagonal instability develops spontaneously: pores that are too close experience excess repulsive stress that drives them outward, while pores that are too far experience reduced stress that allows them to drift inward. Under CC anodizing at a non-optimal voltage, the self-ordering driving force is reduced. GPC can incorporate a deliberate low-current phase corresponding to the optimal ordering voltage in each pattern cycle, providing periodic reinforcement of the ordering instability [9, 15].

2.4 Characteristic Timescales and the Basis for GPC Pattern Period Selection

A critical question for any temporally structured anodizing protocol is whether the pattern period T is commensurate with the physical timescales of the processes being controlled. Three distinct characteristic timescales govern anodizing, and they differ by orders of magnitude: the thermal relaxation timescale $\tau_{thermal}$ (the time for Joule-heated oxide to equilibrate with the electrolyte after a current reduction), the electrochemical kinetic timescale $\tau_{kinetic}$ (the time for the formation–dissolution balance to re-equilibrate following a current step), and the self-ordering timescale τ_{order} (the time for pore positions to relax toward hexagonal equilibrium under mechanical stress).

Thermal relaxation in the oxide–electrolyte system is governed by the thermal diffusivity of the electrolyte and the oxide layer thickness. For typical hard anodizing

conditions (sulfuric acid at 0–5°C, oxide layer 10–50 μm), heat generated in the oxide dissipates into the electrolyte on a timescale $\tau_{thermal} \approx d^2_{oxide} / \alpha_{electrolyte} \approx 1–30$ seconds, where $\alpha_{electrolyte} \approx 1.4 \times 10^{-7}$ m²/s is the thermal diffusivity of dilute sulfuric acid. The electrochemical kinetic timescale $\tau_{kinetic}$ for re-equilibration of the field-assisted ionic transport following a current step is determined by the barrier layer capacitance and the cell resistance: $\tau_{kinetic} = R_{cell} \cdot C_{barrier} \approx 10–300$ seconds for typical anodizing conditions [14, 16]. The self-ordering timescale τ_{order} for long-range hexagonal ordering is substantially longer: experimental observations of AAO self-ordering in oxalic acid at 40 V place τ_{order} in the range of 10–60 minutes for ordering domains of several micrometres [2, 9, 10, 15].

This timescale separation is the key that makes GPC pattern period selection tractable rather than arbitrary. The three phases of the GPC pattern are designed to address processes at three distinct timescales: the low-current relaxation phase (duration $t_{low} \geq \tau_{thermal}$, typically 10–60 seconds) addresses thermal equilibration; the mid-current balance phase (duration $t_{mid} \geq \tau_{kinetic}$, typically 30–300 seconds) addresses formation–dissolution re-equilibration; and the full pattern period T (typically 1–10 minutes, chosen as a fraction of τ_{order}) provides periodic reinforcement of the self-ordering instability over the longer ordering timescale. Because $\tau_{thermal} \ll \tau_{kinetic} \ll \tau_{order}$, the three mechanisms can be addressed within a single hierarchical pattern period without interference between timescales. Critically, these pattern periods (minutes) are far slower than the sub-second pulse durations used in conventional pulse anodizing, and are entirely consistent with the temporal resolution of standard programmable anodizing rectifiers.

The timescale argument also clarifies the distinction between GPC and conventional pulse anodizing. Pulse anodizing typically operates at pulse periods of milliseconds to seconds, which is below $\tau_{kinetic}$ and therefore cannot influence the formation–dissolution balance or self-ordering kinetics; its benefit is limited to thermal management through rapid duty-cycle averaging of Joule heating. GPC operates at pattern periods that are commensurate with or longer than $\tau_{kinetic}$ and a rational fraction of τ_{order}, enabling mechanistic control over all three phenomena simultaneously. This distinction is fundamental: GPC is not a faster or more sophisticated pulse protocol—it is a qualitatively different approach to temporal current design based on explicit matching of pattern structure to process timescales.

2.5 Joule Heating and the Burning Threshold

The power dissipated in the oxide layer per unit area is:

$$P_{Joule} = j^2 \cdot R_{oxide} = j \cdot V_{oxide}$$

For hard anodizing in oxalic or sulfuric acid at low temperature (0–5°C), Joule heating at $j > 50–80$ mA/cm² can cause local temperature increases of 5–15°C within the oxide layer [6, 7]. When the local temperature exceeds the dissolution–formation crossover temperature, the dissolution rate exceeds the formation rate and burning propagates laterally—destroying the anodic film. Since $P_{Joule} \propto j^2$, GPC's periodic low-current relaxation intervals reduce the time-averaged Joule heating below the CC value at the same average j, raising the effective burning threshold.

3. Three GPC Oxide Morphology Control Mechanisms

3.1 Formation-Dissolution Balance Control

GPC's three-phase pattern provides independent control over the formation and flow phases within each cycle. During the high-current phase (Ihigh, duration thigh), the electric field across the barrier layer is elevated, driving rapid field-assisted Al^{3+} migration and oxide formation at maximum rate. During the mid-current phase (Imid ≈0.4–0.6·Ihigh, duration tmid), the field drops below the fast-growth threshold but remains sufficient to maintain the pore structure. During the low-current phase (Ilow ≈0.05–0.15·Ihigh, duration tlow), both formation and viscous flow are minimized, allowing the oxide to consolidate and the local temperature to decrease.

Jensen's inequality applied to the exponential field-assisted formation kinetics confirms that the time-averaged formation rate under GPC differs from the formation rate at the time-averaged current:

$$\langle R_{form}(I(t)) \rangle \neq R_{form}(\langle I \rangle)$$

For the exponential high-field transport law, Rform is convex in j, so the time-averaged formation rate under GPC exceeds that under CC at the same average j during the high-current phase—providing a higher instantaneous formation rate with lower time-averaged thermal load, improving current efficiency and pore morphology definition.

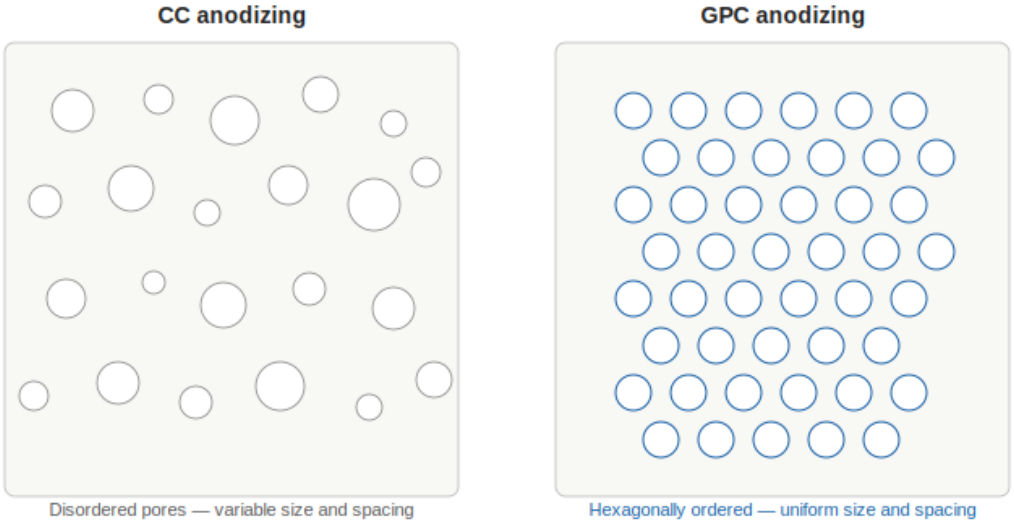

Figure 1. *Anodic alumina pore arrangement (top view schematic): CC anodizing (left, disordered pores with variable diameter and irregular spacing) vs GPC anodizing (right, hexagonally ordered pores with uniform diameter distribution).*

3.2 Pore Self-Ordering Enhancement

The self-ordering kinetics mechanism exploits the relationship between anodizing voltage and the mechanical stress field that drives hexagonal pore ordering. At the optimal anodizing voltage Vopt for a given electrolyte-temperature combination (Vopt ≈25 V in sulfuric acid, ≈40 V in oxalic acid, ≈195 V in phosphoric acid [2, 9, 10]), the hexagonal instability is strongest and self-ordering proceeds at maximum rate.

GPC can incorporate a deliberate low-current phase at Iopt = Vopt/Rcell in each pattern cycle, providing a recurring interval during which the ordering instability is activated and pore

positions are reinforced. The optimal frequency for this self-ordering phase is related to the pore-ordering time constant:

$$f_{opt} \approx 0.1–0.3 / \tau_{order}$$

For typical AAO in oxalic acid at 40 V, GPC pattern periods of 1–10 minutes provide the periodic reinforcement that accumulates toward macroscopic hexagonal order, analogous to the mechanical vibration applied in some experimental self-ordering studies but implemented entirely through current temporal structure [9, 15].

3.3 Thermal Stabilization and Burning Prevention

The time-averaged Joule heating under GPC is:

$$\langle P_{Joule} \rangle_{GPC} = I_{high}^2 \cdot R \cdot t_{high}/T + I_{mid}^2 \cdot R \cdot t_{mid}/T + I_{low}^2 \cdot R \cdot t_{low}/T$$

where T = thigh + tmid + tlow is the pattern period. Since PJoule ∝ I², the low-current phase contributes negligibly to average Joule heating while providing substantial thermal recovery time. GPC's periodic low-current relaxation intervals effectively decouple the peak formation rate (set by Ihigh) from the time-averaged thermal load (set by the pattern duty cycle).

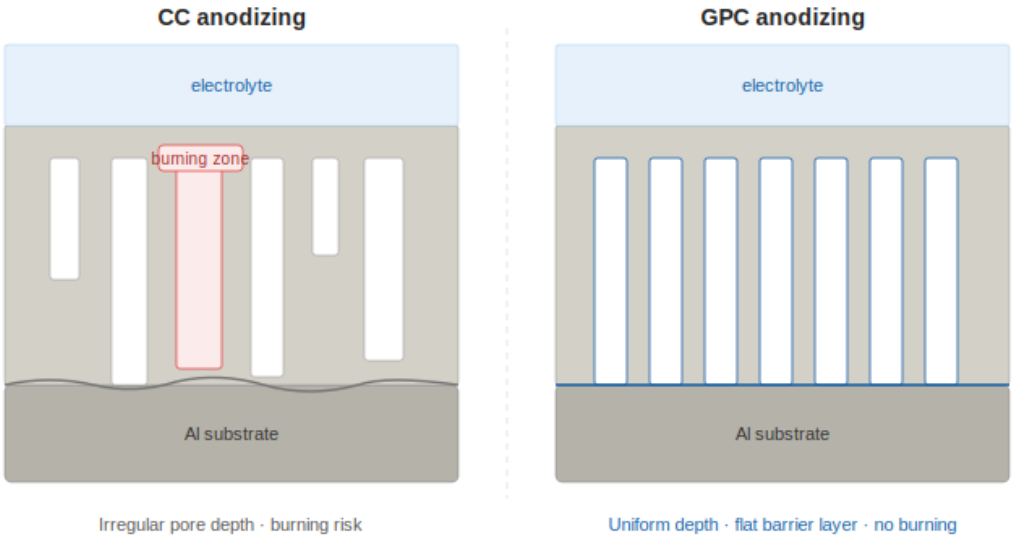

Figure 2. *Anodic oxide cross-section schematic (side view): CC anodizing (left) showing irregular pore depth, variable wall thickness, and burning zone; GPC anodizing (right) showing uniform pore depth, controlled flat barrier layer, and thermal stabilization through low-current relaxation phases.*

4. GPC Anodizing Protocol Design

4.1 Three-Phase Current Architecture

The GPC anodizing protocol integrates the three morphology control mechanisms into a composite three-phase current profile:

$$I(t) = I_{high}\ [\text{oxide growth, } t_{high}] \rightarrow I_{mid}\ [\text{dissolution balance, } t_{mid}] \rightarrow I_{low}\ [\text{thermal relax + ordering, } t_{low}]$$

Protocol parameter selection proceeds from characterization of the target system. The optimal anodizing voltage Vopt and its corresponding current density Iopt = Vopt/Rcell are determined from the literature or a brief CC sweep. Ihigh is set to achieve the maximum desired oxide growth rate while keeping the peak Joule temperature below the burning threshold. Imid

is set at Vopt/Rcell for self-ordering reinforcement. Ilow is set to 5–15% of the mean current for thermal recovery. The pattern period T is set by the self-ordering time constant divided by 3 to provide multiple self-ordering reinforcement cycles per ordering time constant.

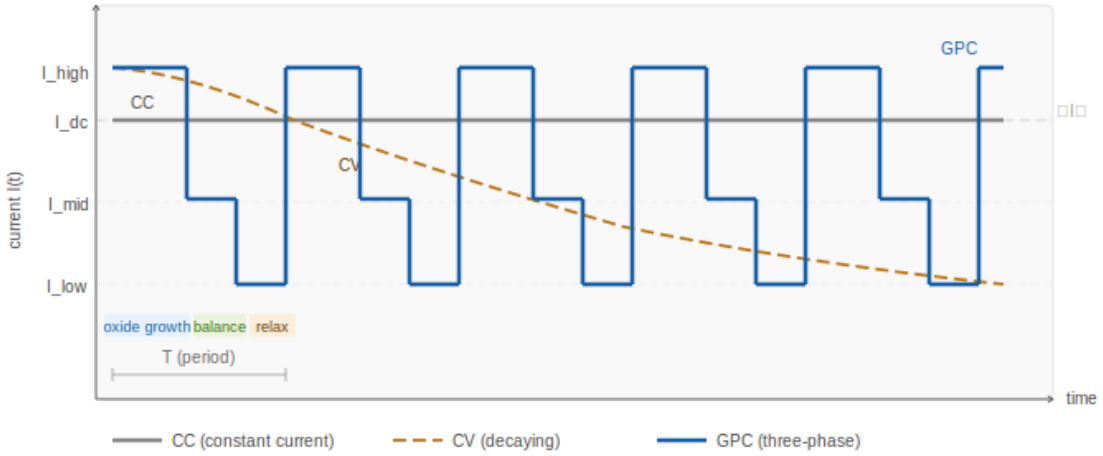

Figure 3. *Current profile comparison: CC anodizing (gray, constant at I_dc), CV (amber dashed, decaying), and GPC three-phase pattern (blue). The GPC pattern alternates between high-current oxide growth phase, mid-current dissolution balance and self-ordering phase, and low-current thermal relaxation phase. All three profiles share the same mean current ⟨I⟩. T denotes one GPC pattern period.*

4.2 GigaPulse Lab Reference Implementation

The GigaPulse Lab platform serves as the reference implementation for GPC anodizing. GP Lab connects to the I and V control input terminals of the existing anodizing power supply—no hardware replacement is required. The power supply applies the current pattern to the anodizing cell; the cell connects only to the power supply output terminals and not directly to GP Lab. Real-time feedback—measured current I, voltage V, cell temperature T, and oxide voltage Voxide—returns from the power supply to GP Lab for closed-loop control.

The platform's real-time analysis module tracks Voxide evolution (which reflects the growing barrier layer resistance), computes the thermal index from $I^2 \cdot Rcell$ as an estimate of instantaneous Joule heating, and monitors dVoxide/dt as an indicator of formation-dissolution balance. The decision engine implements an adaptive burning prevention protocol: when the thermal index exceeds a threshold corresponding to jburn, the low-current phase is extended until the thermal index drops below a safe level.

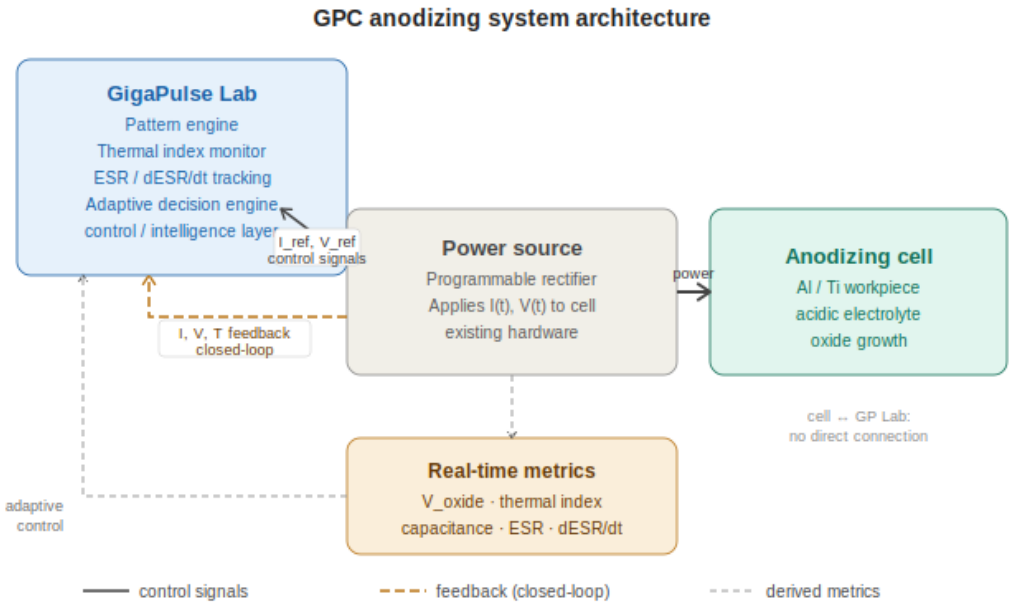

Figure 4. *GPC anodizing system architecture. GigaPulse Lab (left) connects to Power Source I and V control input terminals—no hardware replacement required. Power Source applies current pattern to the Anodizing Cell; cell connects to Power Source output only. Real-time feedback (I, V, T) from Power Source to GP Lab enables closed-loop thermal index monitoring. Real-time metrics (Voxide, thermal index, ESR) are computed and fed to the adaptive decision engine.*

5. Technology-Specific Considerations

5.1 Aluminum Anodizing (AAO Template Fabrication)

Aluminum anodizing for AAO template fabrication requires long-range hexagonal ordering over areas of cm² or larger. The standard two-step anodizing process—a first anodizing step to establish hexagonally ordered bottom surface features, followed by chemical removal of the first oxide and a second anodizing step that nucleates pores at the ordered surface features—relies on self-ordering during the first step to produce sufficient template regularity [2, 5]. GPC's self-ordering enhancement mechanism directly improves the quality of the first-step template.

The viscous flow model [26] predicts that the oxide porosity and pore wall density are sensitive to the history of the formation rate at the barrier layer. A GPC pattern that applies a higher instantaneous formation rate during Ihigh phases produces denser, more mechanically robust pore walls compared to CC at the same average j—which is directly relevant to AAO membrane applications requiring high aspect ratio pores without wall collapse.

5.2 Titanium Anodizing (TiO_2 Nanotube Arrays)

Titanium anodizing in fluoride-containing electrolytes produces TiO_2 nanotube arrays through a mechanism in which fluoride ions complex Ti^{4+} at the tube bottom, enabling chemical dissolution of TiO_2 to form hollow tubes [27]. Li et al. [28] clarified that the pore growth rate is controlled primarily by the oxide formation rate at the barrier layer; an analogous relationship is expected for TiO_2 nanotube growth.

The formation-dissolution balance in titanium anodizing is particularly sensitive to local temperature because the fluoride-mediated dissolution rate has a higher thermal activation

than the field-assisted formation rate [27]. GPC's thermal stabilization mechanism is therefore proportionally more beneficial for TiO_2 nanotube formation than for AAO. The Pilling–Bedworth ratio for Ti/TiO_2 (≈2.5) is larger than for Al/Al_2O_3 (≈1.3), suggesting stronger stress-driven ordering forces that may make GPC's self-ordering phase particularly effective for producing ordered TiO_2 nanotube arrays.

6. Expected Outcomes

The GPC anodizing efficiency factor for morphology control is defined as:

$$\Psi_{GP,anod} = \theta_{hex,GPC} / \theta_{hex,CC}$$

where θhex is the fraction of hexagonally coordinated pores determined from fast Fourier transform analysis of scanning electron microscopy top-view images. From the self-ordering kinetics analysis in Section 3.2, a value of ΨGP,anod = 1.2–1.5 is predicted, representing 20–50% improvement in ordering degree for equal anodizing time. Table 1 summarizes the predicted outcomes.

Parameter	CC anodizing	GPC anodizing
Pore ordering degree (θhex)	Reference	↑ 20–50% improvement
Pore diameter coefficient of variation	Reference (broad)	↓ Narrowed distribution
Burning threshold (j_burn)	Reference	↑ Higher effective threshold
Hard anodizing growth rate	Reference (limited by j_burn)	↑ Increased
Total oxide thickness	Reference	Preserved (same ⟨I⟩)
Current efficiency	Reference	↑ Improved
ΨGP,anod ordering factor	1.0	1.2–1.5×

Table 1. *Predicted GPC anodizing outcomes compared to CC baseline at equal average current density and equal total oxide thickness.*

7. Experimental Validation Framework

7.1 Proposed Protocol

Independent experimental validation requires parallel comparison of CC and GPC anodizing protocols applied to identical aluminum or titanium samples with equal average current density and equal total charge passed. The primary measurement suite includes: pore arrangement characterization by scanning electron microscopy top-view imaging with fast Fourier transform analysis for ordering degree; pore diameter distribution from scanning electron microscopy image analysis; oxide thickness from cross-section scanning electron microscopy; barrier layer thickness from transmission electron microscopy or electrochemical impedance spectroscopy; and current efficiency from gravimetric oxide weight measurement versus Faradaic prediction.

Aluminum anodizing in 0.3 M oxalic acid at 40 V provides a well-characterized model system with established self-ordering literature [2, 4, 9, 10]. Hard anodizing of aluminum in 10–20 wt% sulfuric acid at −5 to 0°C provides the most relevant validation for the burning prevention mechanism. For titanium, anodizing in ethylene glycol containing 0.3 wt% ammonium fluoride and 2 vol% water at 60 V constitutes a standard nanotube formation protocol [5, R2] against which GPC performance can be compared.

7.2 GigaPulse Lab Integration

GPC anodizing is directly implementable on existing anodizing equipment without modification of the anodizing tank, electrolyte, or workpiece fixturing. GP Lab connects to the I and V control terminals of the existing rectifier. For laboratory-scale validation, a standard potentiostat/galvanostat is compatible; for industrial-scale validation, any programmable rectifier with setpoint input accepts GP Lab control signals. The thermal index monitoring capability of GP Lab provides real-time burning prevention that protects both the workpiece and process equipment during validation at elevated current densities.

8. Discussion

8.1 Implications of the Viscous Flow Model for GPC Design

The viscous flow model of pore growth [26] has direct implications for GPC protocol design that were not apparent under the classical field-assisted dissolution model. A GPC pattern that alternates between high and low formation rates may produce pore walls with a controlled density gradient—denser at the outer wall surface (formed during the consolidation phase) and more porous at the barrier layer interface (formed during the high-current phase). This layered wall structure could improve the mechanical robustness of high-aspect-ratio AAO membranes.

8.2 Scope of the Theoretical Claims and the Role of Experimental Verification

The claims made in this paper are theoretical in character: they derive from the mathematical properties of Jensen's inequality applied to the nonlinear kinetics established in the referenced literature, from the timescale analysis of Section 2.4, and from the mechanistic framework of the viscous flow model [26] and the fluoride dissolution studies [27, 28]. The paper does not claim that GPC has been experimentally demonstrated to improve pore ordering or oxide morphology—it claims that the underlying physical mechanisms provide a rigorous theoretical basis for expecting such improvements, and that the experimental validation framework of Section 7 constitutes a direct test of the predictions.

The theoretical argument has a specific logical structure that distinguishes it from speculative conjecture. First, it is established that pore ordering is a kinetic process driven by the mechanical stress instability that operates on the timescale τ_{order} [4, 9, R1]. Second, it is established that the strength of the ordering instability depends on the anodizing voltage, with a well-defined optimal voltage Vopt for each electrolyte-temperature combination [2, 9, 10]. Third, it is established that GPC can deliver a periodic phase at Vopt within each pattern cycle without disrupting the mean current or total oxide thickness. The logical conclusion—that periodic reinforcement of the ordering instability at its optimal conditions should accelerate

ordering compared to CC at a non-optimal voltage—follows from these three established facts. Whether the predicted improvement of $\Psi_{GP,anod}$ = 1.2–1.5× is quantitatively accurate requires experimental measurement; whether the qualitative direction of the effect is correct is a consequence of the physical model, not an assumption.

It is also worth noting that the referenced literature itself provides indirect support for the temporal current structuring concept. Garcia-Vergara et al. [26] demonstrated that oxide formation rate at the barrier layer—not dissolution at the pore tip—is the dominant kinetic variable in pore growth; this means modulating the formation rate through temporal current structuring is modulating the primary control variable of the system. Zhuang et al. [27] showed that fluoride-mediated dissolution in TiO_2 nanotube formation is thermally activated to a high degree; this means reducing time-averaged Joule heating through GPC thermal stabilization reduces the dominant dissolution pathway. Li et al. [28] confirmed that pore growth rate scales with barrier layer formation rate; this means the GPC high-current phase directly accelerates the rate-limiting step. These results collectively support rather than contradict the mechanistic basis of the GPC approach, even though they were not originally motivated by temporal current structuring.

8.3 GPC vs Two-Step Anodizing

The established method for achieving high-quality AAO ordering is the two-step anodizing process [2, 5]: a first long anodizing step (often 12–24 hours) establishes hexagonally ordered surface imprints, the first oxide is removed chemically, and the second anodizing step nucleates at the ordered imprints. GPC's self-ordering enhancement offers an alternative pathway: by periodically reinforcing the self-ordering instability through the optimal-voltage phase in each pattern cycle, GPC may accelerate the development of hexagonal order during the first anodizing step, potentially reducing the first-step duration and eliminating the intermediate chemical etching step with its associated environmental impact.

8.4 GPC Anodizing in the Context of the Electrochemical Series

GPC anodizing shares the core Jensen inequality mechanism with all other GPC electrochemical applications in this series [1, 26–33]: nonlinear electrochemical kinetics respond differently to temporally structured current than to equivalent constant current. In anodizing, the nonlinearity arises from the exponential field-assisted transport in the barrier layer—more nonlinear than the Butler–Volmer kinetics in plating and electrolysis—suggesting that GPC's morphological benefit may be proportionally larger in anodizing than in other application domains analyzed in this series.

9. Conclusion

This paper has established the theoretical framework for applying Generated Pattern Current (GPC) to anodizing of aluminum and titanium, incorporating the viscous flow model [26] and the fluoride-mediated dissolution mechanism [27, 28] as the governing physical framework. The three concurrent phenomena that limit CC and CV anodizing—formation-dissolution balance, pore self-ordering kinetics, and Joule heating—can be independently addressed through GPC's three-phase temporal current design: high-current oxide growth,

mid-current dissolution balance at the optimal ordering voltage, and low-current thermal relaxation.

Jensen's inequality applied to the exponential field-assisted oxide formation kinetics formally establishes that temporally structured current produces different time-averaged oxide morphology than equivalent CC. The total oxide volume grown depends only on the total charge passed by Faraday's law, so GPC preserves oxide thickness at equal average current while improving ordering degree by a predicted factor of 1.2–1.5×, narrowing pore diameter distribution, suppressing burning, and enabling higher growth rates in hard anodizing.

The GigaPulse Lab platform provides immediate deployment capability on existing anodizing equipment without hardware replacement. The experimental validation framework proposed in Section 7 is designed to be implementable with standard anodizing and characterization equipment, providing a clear path to quantitative verification of the predicted GPC advantages.

References

[1] I. Karakoc, "Dynamic Defined Pattern Charging (DDPC)," PCT/TR2025/051176; USPTO 19/298,223. Priority: July 23, 2025.

[2] H. Masuda and K. Fukuda, "Ordered Metal Nanohole Arrays Made by a Two-Step Replication of Honeycomb Structures of Anodic Alumina," Science, vol. 268, pp. 1466–1468, 1995.

[3] J. P. O'Sullivan and G. C. Wood, "Morphology and Mechanism of Formation of Porous Anodic Films on Aluminium," Proc. R. Soc. London A, vol. 317, pp. 511–543, 1970.

[4] O. Jessensky, F. Muller, and U. Gosele, "Self-Organized Formation of Hexagonal Pore Arrays in Anodic Alumina," Appl. Phys. Lett., vol. 72, pp. 1173–1175, 1998.

[5] W. Lee and S. J. Park, "Porous Anodic Aluminum Oxide: Anodization and Templated Synthesis of Functional Nanostructures," Chem. Rev., vol. 114, pp. 7487–7556, 2014.

[6] W. Lee, R. Ji, U. Gosele, and K. Nielsch, "Fast Fabrication of Long-Range Ordered Porous Alumina Membranes by Hard Anodization," Nat. Mater., vol. 5, pp. 741–747, 2006.

[7] G. E. Thompson, "Porous Anodic Alumina: Fabrication, Characterisation and Applications," Thin Solid Films, vol. 297, pp. 192–201, 1997.

[8] K. Nielsch, R. B. Wehrspohn, J. Barthel, J. Kirschner, U. Gosele, S. F. Fischer, and H. Kronmuller, "Uniform Nickel Deposition into Ordered Alumina Pores by Pulsed Electrodeposition," Adv. Mater., vol. 12, pp. 582–586, 2000.

[9] H. Masuda, H. Yamada, M. Satoh, H. Asoh, M. Nakao, and T. Tamamura, "Highly Ordered Nanochannel-Array Architecture in Anodic Alumina," Appl. Phys. Lett., vol. 71, pp. 2770–2772, 1997.

[10] A. P. Li, F. Muller, A. Birner, K. Nielsch, and U. Gosele, "Hexagonal Pore Arrays with a 50–420 nm Interpore Distance," J. Appl. Phys., vol. 84, pp. 6023–6026, 1998.

[11] S. Z. Chu et al., "Highly Porous (TiO2–SiO2–TeO2)/Al2O3/TiO2 Composite Nanostructures on Glass with Optical and Photocatalytic Properties," J. Phys. Chem. B, vol. 107, pp. 6586–6589, 2003.

[12] G. D. Sulka, "Highly Ordered Anodic Porous Alumina Formation by Self-Organized Anodizing," in Nanostructured Materials in Electrochemistry, A. Eftekhari, Ed. Wiley-VCH, 2008.

[13] F. Keller, M. S. Hunter, and D. L. Robinson, "Structural Features of Oxide Coatings on Aluminum," J. Electrochem. Soc., vol. 100, pp. 411–419, 1953.

[14] V. P. Parkhutik and V. I. Shershulsky, "Theoretical Modelling of Porous Oxide Growth on Aluminium," J. Phys. D: Appl. Phys., vol. 25, pp. 1258–1263, 1992.

[15] S. Ono, M. Saito, M. Ishiguro, and H. Asoh, "Controlling Factor of Self-Ordering of Anodic Porous Alumina," J. Electrochem. Soc., vol. 151, pp. B473–B478, 2004.

[16] A. J. Bard and L. R. Faulkner, Electrochemical Methods: Fundamentals and Applications, 2nd ed. New York: Wiley, 2001.
[17] J. Newman and K. E. Thomas-Alyea, Electrochemical Systems, 3rd ed. Hoboken: Wiley, 2004.
[18] M. Schlesinger and M. Paunovic, Eds., Modern Electroplating, 5th ed. Hoboken: Wiley, 2010.
[19] N. Ibl, "Some Theoretical Aspects of Pulse Electrolysis," Surface Technol., vol. 10, pp. 81–104, 1980.
[20] M. S. Chandrasekar and M. Pushpavanam, "Pulse and Pulse Reverse Plating," Electrochim. Acta, vol. 53, pp. 3313–3322, 2008.
[21] H. Vogt and R. J. Balzer, "The Bubble Coverage of Gas-Evolving Electrodes in Stagnant Electrolytes," Electrochim. Acta, vol. 50, pp. 2073–2079, 2005.
[22] P. Roy, S. Berger, and P. Schmuki, "TiO2 Nanotubes: Synthesis and Applications," Angew. Chem. Int. Ed., vol. 50, pp. 2904–2939, 2011.
[23] H. Tsuchiya and P. Schmuki, "Less Ordered Titanium Dioxide Nanotubes by Anodization," Electrochem. Commun., vol. 6, pp. 1131–1134, 2004.
[24] A. Ghicov and P. Schmuki, "Self-Ordering Electrochemistry: A Review on Growth and Functionality of TiO2 Nanotubes," Chem. Commun., pp. 2791–2808, 2009.
[25] R. Beranek, H. Hildebrand, and P. Schmuki, "Self-Organized Porous Titanium Oxide in H2SO4/HF Electrolytes," Electrochem. Solid-State Lett., vol. 6, pp. B12–B14, 2003.
[26] S. J. Garcia-Vergara, P. Skeldon, G. E. Thompson, and H. Habazaki, "A Flow Model of Porous Anodic Film Growth on Aluminium," Electrochim. Acta, vol. 52, pp. 681–687, 2006.
[27] Y. Zhuang, Y. Zhou, T. Zhang, and X. Ma, "Real Role of Fluoride Ions in the Growth of Anodic TiO2 Nanotubes," J. Phys. Chem. C, vol. 128, pp. 5741–5748, 2024.
[28] P. Li, Y. Liu, S. Zheng, and W. Liang, "What Factors Determine the Pore Growth Rate of Porous Anodic Alumina?," Nanotechnology, vol. 37, p. 065602, 2026.
[29] I. Karakoc, "Generated Pattern Current for Battery Formation: SEI Structuring and Electrochemical Efficiency," SSRN Preprint, 2025.
[30] I. Karakoc, "Generated Pattern Current for Battery Optimization: Cycle Performance and Degradation Reduction," SSRN Preprint, 2025.
[31] I. Karakoc, "Generated Pattern Current for First Charge: Controlled Activation of Lithium-Ion Cells," SSRN Preprint, 2025.
[32] I. Karakoc, "Generated Pattern Current for Electroplating: Grain Refinement and Deposit Morphology Control," SSRN 6439004, 2026.
[33] I. Karakoc, "Generated Pattern Current for Water Electrolysis: Bubble Management and Faradaic Efficiency Enhancement," SSRN Preprint, 2026.
[34] I. Karakoc, "Generated Pattern Current for Electro-Dissolution: Precision Material Removal and Surface Finish," SSRN Preprint, 2026.
[35] I. Karakoc, "Generated Pattern Current for Graphene Exfoliation: Controlled Interlayer Expansion and Defect Management," SSRN 6451578, 2026.
[36] I. Karakoc, "GPC Framework: A Universal Electrochemical Process Control Paradigm," SSRN 6387818, 2025.

Acknowledgments

The GPC-based anodizing protocol is protected under PCT/TR2025/051176 and USPTO Application No. 19/298,223. The author is the named inventor. No external funding was received for the preparation of this manuscript.

Declaration of Competing Interest

Ibrahim Karakoc holds the intellectual property and commercial rights related to the Generated Pattern Current (GPC) and Dynamic Defined Pattern Charging (DDPC) technology described in this paper.

Data Availability

Data will be made available on request.

Declaration on Use of AI Writing Assistance

The author used an AI language assistant for manuscript preparation and English language refinement. The author is fully responsible for all scientific content and conclusions presented in this manuscript.